Ethiopian Journal of Natural and computational Science(EJNCS)

Ethiop J Nat Comp Sci 2026, Volume 6, Issue 1

Original Research Article

IMEX Runge-Kutta time-integrators for air-pollution tracking model

J.O. Ehigiea, [1,*],F.C. Ndubuogaranya[1], O.J. Odueso [2] E.O. Ayeni[1], S.A. Okunuga[1]

1 Department of Mathematics, University of Lagos, Nigeria

2 Department of Software Engineering, University of Staffordshire, United Kingdom

* Correspondence: jehigie@unilag.edu.ng

Article History:
Received: 15 July 2025
Accepted: 20 September 2025
Published : 10 February 2026

ABSTRACT

This study investigates the application of Implicit–Explicit Runge–Kutta (IMEX-RK) methods for the numerical simulation of air pollution tracking models. These models, governed by advection–diffusion–reaction (ADR) equations, play a vital role in predicting the dispersion and concentration of pollutants in the atmosphere. Conventional numerical methods often struggle to efficiently and accurately solve ADR equations, particularly in the presence of stiff components. The IMEX-RK framework overcomes these challenges by treating the stiff components implicitly while handling the non-stiff components explicitly. In this work, a class of IMEX-RK schemes is developed and analysed, including the IMEX Trapezoidal Method (`IMEX2s2`) and third-order variants (`IMEX3s3`). Their corresponding stability regions are also presented. Numerical simulations demonstrate the capability of these schemes to capture pollutant transport dynamics with high accuracy under varying advection and diffusion parameters. Furthermore, the accuracy of the proposed IMEX-RK methods are assessed, and results show that both `IMEX2s2` and `IMEX3s3` methods accurately reproduce pollutant concentration profiles, with the `IMEX3s3` scheme exhibiting superior accuracy compared to the `IMEX2s2` and a diagonal implicit Runge-Kutta method in the literature.

Keywords: Implicit-Explicit Runge-Kutta methods, Advection-Diffusion-Reaction, Air-Pollution,Runge-Kutta methods, Rooted tree

1 Introduction

1.1 Air pollution tracking model

The dynamics of these toxic pollutant materials over time can be tracked using mathematical models known as Advection-Diffusion-Reaction (ADR) equations. The ADR is a partial differential equation that describes physical phenomena where particles, energy, or other physical quantities are transferred inside a physical system due to two processes—diffusion and advection, see Rubin (2001). It is a mathematical model that has been used to model the concentration of pollutants. Advection is first due to the movement of materials from one region to another and diffusion is due to the movement of materials from higher concentration to low concentration. ADR equations give the amount of pollutant concentration fields after input of the velocity data from the hydrodynamic model which are derived from mass balances. Formally, the ADR equation is given by:

$$\frac{\partial \varphi}{\partial t} + \nabla \cdot (\mathbf{v}\varphi) + \nabla \cdot (D\nabla\varphi) + \sigma\varphi = R(\varphi) \tag{1.1}$$

where:

- φ represents the concentration of the pollutant
- $\mathbf{v}$ represents the wind or drift velocity field
- D is the diffusion coefficient, and
- $R(\varphi)$ is the reaction or source function that describes where the pollutant material is generated and its power

The ADR model is a widely used PDEs for simulating the transport, diffusion and transformation of pollutants materials in the atmosphere. An extensive application of nonlinear PDEs in environmental fluid dynamics are discussed in Rubin (2001). Traditional numerical methods, including finite difference and finite element methods, have been applied to solve air-pollution models. However, these methods can struggle with the stiff nature of the equations, particularly when modelling rapid chemical reactions or complex interactions between pollutants and meteorological factors, see Dang and Ehrhardt (2006). Researchers from Bulgaria, Sweden and Vietnam have made notable contributions in developing numerical method for simulating air-pollution tracking. In

Bulgaria, Vulkov and co-workers explored operator splitting approach in tackling the ADR equations, see Dimov et al (2017). Meanwhile, In Vietnam, Dang's lab incorporated optimal control to the ADR to improve the predictive capabilities with the aim of some constraints relevant to localized environmental conditions, see Dang et al. (2007). In Sweden, Zlatev research group contributed to global and regional air-pollution modelling by emphasizing the use of High-Performance computing implementations, see Georgiev et al. (2023).

Explicit Runge-Kutta methods are widely used in the numerical simulation of time-dependent PDEs. However, explicit methods are limited by small timestep which makes implementation computationally expensive and may not be suitable for real-time air-pollution calculations. Robust and innovative time-integrators have been proposed to improve computational efficiency and accuracy, see Butcher (2016). Implicit-Explicit (IMEX) schemes, which treat stiff and non-stiff components differently, have gained significant attention. The IMEX Runge-Kutta methods have been shown to handle the challenges posed by the advection-diffusion-reaction (ADR) equations effectively, see Asher et al. (1997). A positivity preserving finite difference schemes for air-pollution tracking using the ADR was developed by Habingabwa (2012). In this paper, the method of lines is used for semi-discretization to obtain the semi-discrete formulation of the ADR. This procedure replaces spatial partial derivatives in the ADR with symmteric difference approximations numerically. Consequently, a large system of ordinary differential equations with one independent variable t are obtained. The semi-discrete formulation (**??**) arising in practical applications is often highly nonlinear.

Recent advances in air pollution modelling have combined developments in numerical analysis, computational methods, and artificial intelligence to enhance both accuracy and interpretability. Rodrigo Bonet (2024) proposed several graph-based deep learning frameworks that integrate physics-guided learning and explainable AI to infer and interpret pollutant dynamics more effectively. In a related direction, Salman (2024) developed advanced deep learning architectures for model emulation and uncertainty-aware air quality forecasting, extending the use of data-driven methods in environmental modelling. Using numerical analysis, Zlatev et al. (2022) focused on the efficient numerical treatment of atmospheric chemical schemes using Implicit Runge–Kutta methods combined with advanced Richardson Extrapolation, while Karátson and Kovács (2016) employed finite element approaches and parallel computation for nonlinear parabolic systems arising in pollution transport. Yang et al. (2019) modelled urban air pollution due

to vehicular emissions using a continuum approach, solving the conservation and advection–diffusion equations with a high-order WENO and TVD Runge–Kutta scheme. Liang et al. (2025) extended this numerical frontier with a fourth-order cut-cell method for advection–diffusion problems involving moving boundaries, addressing discontinuities through a robust cell-merging technique. Similarly, Ahmad et al. (2025) applied the CFD tool MGLET to simulate pollutant dispersion in urban Munich, capturing complex flow structures such as street-canyon recirculation zones. In a different but complementary study, Shettar et al. (2024) examined the role of magnetised nanoparticle aggregation in pollutant transport across a stretching disc using the Runge–Kutta–Fehlberg method. Finally, Wang et al. (2022) introduced a deep residual neural network emulator for gas-phase chemical kinetics, significantly accelerating the most computationally intensive component of global air quality models. Collectively, these studies highlight the trend towards hybrid frameworks that combine physical modelling, numerical accuracy, and machine learning to achieve efficient and interpretable air pollution prediction.

Conventional explicit time-integration methods are unsuitable for such problems due to severe stability-induced restrictions on the allowable time step. Although implicit schemes, such as Diagonally Implicit Runge–Kutta (DIRK) methods, can circumvent these restrictions, their implementation typically requires solving the entire nonlinear system at each step, resulting in considerable computational expense. To address this challenge, we adopt a splitting strategy in which the system is decomposed into its stiff and non-stiff components. An implicit–explicit Runge–Kutta (IMEX-RK) framework is then constructed such that the explicit part advances the non-stiff component, while the implicit part is applied to the stiff component. This partitioning confines the nonlinear treatment to a reduced subset of the system, thereby enhancing computational efficiency without compromising stability.

The paper is organised as follows. Section 2 presents the preliminaries, including the spatial discretization and semi-discrete formulation of the advection–diffusion–reaction (ADR) equation, the IMEX time-integration framework, and the corresponding order conditions. Section 3 describes the derivation of the IMEX Runge–Kutta methods, while Section 4 discusses their stability regions. In Section 5, numerical experiments are provided to demonstrate the performance of the proposed methods on the ADR equations. Finally, Section 6 concludes the paper.

2 Preliminaries

2.1 Spatial and semi-discrete formulation

Consider $\Omega = [0, L] \times [0, L]$, and let $u : \Omega \times (0, \infty) \to (0, \infty)$ be the solution of (**??**). We use a uniform Cartesian grid with nodes (x_i, y_i), where $i, j = 1, \ldots, M$, $x_i = y_i = i\Delta x$ and $\Delta x = L/M$. This results in M^2 grid points, indexed by $\tau = (i, j) \in \mathcal{P}$, with $\mathcal{P} := \{1, \ldots, M\} \times \{1, \ldots, M\} \subset \mathbb{N}^2$. We denote $x_\tau := (x_i, y_j)$ and use two-dimensional unit vectors $e_1 = (1, 0)$ and $e_2 = (0, 1)$ to refer to neighbouring grid points $x_{\tau+e_1} = (x_{i+1}, y_i)$ and $x_{\tau+e_2} = (x_i, y_{j+1})$. We define $u : [0, \infty) \to \mathbb{R}^{M^2}$ as a solution computed at an instant t at the grid points, where $u_\tau(t) = u(x_\tau, t)$ for $\tau \in \mathcal{P}$, see Burger et al. (2020).

Using this notation:

- The advection component is approximated using the symmetric difference scheme:

$$\nabla \cdot (v\phi) = v \cdot \left(\frac{\varphi_{\tau+e_i} - \varphi_{\tau-e_i}}{2\Delta x} \right)$$

- The diffusive component is approximated with the symmetric difference scheme

$$\nabla \cdot (D\nabla\phi) = D \left(\frac{\varphi_{\tau+e_i} - 2\varphi_\tau + \varphi_{\tau-e_i}}{\Delta x^2} \right)$$

Specifically, the resulting system of ODEs for $v = [1, 1]$ takes the form

$$\frac{d\Phi(t)}{dt} = \left(-\frac{A}{2\Delta x}\Phi(t) - \sigma\Phi(t) + R(\Phi) \right) - \frac{D}{\Delta x^2}\Phi(t) = \mathcal{H}(\Phi)$$

with snapshots for matrix A and D given by Figures (**??**).

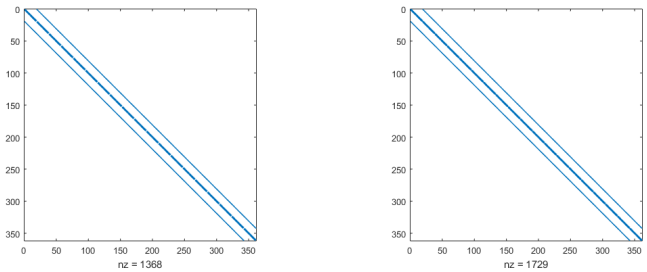

Figure 1: Advection and Diffusion Matrix for $M = 20$

2.2 Time-integration

We seek an approximate solution to a problem that involves a variable (u) that changes over time (t) and follows a specific rule (f), derived from the spatial discretization of the Advection-Diffusion-Reaction (ADR) equation, which models the movement of pollutant materials (**??**). This rule is generally defined by the equation:

$$u' = f(u), \qquad t \geq t_0, u(t_0) = u_0. \tag{2.1}$$

Here, we assume that $f : \mathbb{R}^N \to \mathbb{R}^N$ is a function that satisfies the Lipschitz condition. The initial value problem is defined with the initial condition $u_0 \in \mathbb{R}^N$, which is a given vector and where $\mathbb{R}^d$ denotes the d-dimension real Euclidean space. It is usually assumed that (**??**) has unique solution at $t > 0$ and that $f(u)$ is sufficiently smooth in R^N.

Our objective is to simulate the movement of pollutant materials by approximating the solution of (**??**) using a class of IMEX Runge-Kutta methods. However, we first introduce the Runge-Kutta methods as the time-integrator for solving the resulting system of initial value problems. An s-stage Runge-Kutta (RK) method with timestep Δt for the initial value problem (**??**) is given by

$$\begin{cases} U_i = u_n + \Delta t \sum_{j=1}^{s} a_{ij} f(U_j), & i = 1, ..., s, \\ u_{n+1} = u_n + \Delta t \sum_{i=1}^{s} b_i f(U_i), \end{cases} \tag{2.2}$$

where a_{ij}, b_i, c_i, $i, j = 1, ..., s$ are real constants, $t_n = x_0 + n\Delta t$, Δt is the timestep and $u_n \approx u(t_n), n = 0, 1, \ldots$.

The RK method (**??**) can be represented by the following Butcher tableau:

$$\begin{array}{c|c} c & \mathbf{A} \\ \hline & b^T \end{array} = \begin{array}{c|cccc} c_1 & a_{11} & a_{12} & \cdots & a_{1s} \\ c_2 & a_{21} & a_{22} & \cdots & a_{2s} \\ \vdots & \vdots & \vdots & & \vdots \\ c_s & a_{s1} & a_{s2} & \cdots & a_{ss} \\ \hline & b_1 & b_2 & \cdots & b_s \end{array}, \tag{2.3}$$

where, $b = (b_1, ..., b_s)^T, c = (c_1, ..., c_s)^T$ are s-dimensional vectors and $A = (a_{ij})$ is an $s \times s$ matrix. When the matrix A is strictly lower triangular, i.e,. $a_{ij} = 0$ for all $1 \leq i \leq j \leq s$, the method is *explicit*, otherwise it is *implicit*.

Conventionally, it is assumed that $Ae = c$ with $e = (1, ..., 1)^T$, the $s \times 1$ vector of units, i.e.,

$$c_i = \sum_{j=1}^{s} a_{ij}, \qquad i = 1, ..., s. \tag{2.4}$$

Sometimes, it is convenient to compactly express the RK method (**??**) in block-matrix notation

$$\begin{cases} U = e \otimes u_n + \Delta t(A \otimes I) f(U), \\ u_{n+1} = u_n + \Delta t(b^T \otimes I) f(U), \end{cases} \tag{2.5}$$

where I is the $d \times d$ identity matrix, $\otimes$ is the Kronecker product, $U = (U_1^T, ..., U_s^T)^T$ and $f(U) = f(U_1)^T, ..., f(U_s)^T)^T$. A RK method (**??**) is said to have order p if its local truncation error per step is proportional to Δt^{p+1}, where Δt is the timestep.

2.3 IMEX Runge-Kutta methods

Consider the initial value problem given on the interval $[t_0, t_{end}]$

$$u'(t) = \mathcal{H}(u(t)) = f(u) + g(u), \tag{2.6}$$

where $\mathcal{H}(u(t))$ composed additively of two terms $f(u)$ and $g(u)$. In the IMEX (Implicit-Explicit) formulation for (**??**), an s-stage explicit method is applied to the non-stiff component f, while an s-stage implicit method is applied to the stiff component g. These methods are applied as follows:

$$U_i = u_n + \Delta t \sum_{j=1}^{i-1} a_{ij} f(U_J) + \Delta t \sum_{j=1}^{i} \hat{a}_{ij} g(U_j), \tag{2.7a}$$

$$u_{n+1} = u_n + \Delta t \sum_{j=1}^{s} b_i f(U_i) + \Delta t \sum_{i=1}^{s} \hat{b}_i g(U_i), \tag{2.7b}$$

where a_{ij}, $\hat{a}_{ij}$, b_i and $\hat{b}_i$ are constants, which can be compactly represented by the Butcher matrix form as:

$$\begin{array}{c|c||c} c & A & \hat{A} \\ \hline & b & \hat{b} \end{array} = \begin{array}{c|ccccc||cccc} c_1 & & & & & & & & & \\ c_2 & a_{21} & & & & & a_{21} & a_{22} & & \\ \vdots & \vdots & \ddots & & & & \vdots & \vdots & \ddots & \\ c_s & a_{s1} & \cdots & a_{ss-1} & & & a_{s1} & a_{s2} & \cdots & a_{ss} \\ \hline & b_1 & \cdots & b_{s-1} & b_s & & \hat{b}_1 & \hat{b}_2 & \cdots & \hat{b}_s \end{array} \tag{2.8}$$

.

2.4 Order conditions of IMEX Runge-Kutta methods

To derive the general order conditions, we consider u_{n+1} as the numerical solution at $t_n+\Delta t$, obtained after one step starting from $u(t_n)$, under the local assumption that $u(t_n) = u_n$. We then compare the series expansion of u_{n+1} with that of the exact solution $u(t_n+\Delta t)$.

2.4.1 Expansion of the exact solution

Assume that $\mathcal{H}$ (thus $f(u)$ and $g(u)$) is sufficiently differentiable, its first few higher derivatives, composed of elementary differentials, are given by:

$$\begin{aligned} u' &= \mathcal{H} = f + g \\ u'' &= f'f + f'g + g'f + g'g \\ u''' &= f'f'f + f'f'g + 2f'g'f + 2g'f'g + f''(f,f) + 2f''(f,g) \\ &\quad f''(g,g) + g'g'f + g'g'g + g''(f,f) + 2g''(f,g) + g''(g,g) \end{aligned} \tag{2.9}$$

where f and g and their derivatives are the short abbreviations representing that they are evaluated at u_n. Observe that the expressions for higher derivatives become increasingly very complicated. The p-series discussed in Hairer et al. (2009) introduces a special class of bi-coloured trees. Each term of the right hand side of (**??**) contains elementary differential that can be associated with a class of bi-coloured trees. These trees consist of two types of vertex: black and white, with the following rules:

- f : a terminal black vertex imply the black leaf;
- g : a terminal white vertex imply the white leaf;

- $f^{(k)}(u)$: A black stem that grafts either a black or white leaf or stem with k branches upwards;
- $g^{(k)}(u)$: A white stem that grafts either a black or white leaf or stem with k branches upwards.

The exact solution up to order three is given by:

$$\begin{aligned} u(t_n+\Delta t) &= u_n + \Delta t\mathcal{H} + \frac{\Delta t^2}{2!}(f'f' + f'g + g'f + g'g) \\ &\quad + \frac{\Delta t^3}{3!}\left(\begin{array}{l} f'f'f + f'f'g + 2f'g'f + 2g'f'g + f''(f,f) + 2f''(f,g) \\ f''(g,g) + g'g'f + g'g'g + g''(f,f) + 2g''(f,g) + g''(g,g) \end{array}\right) \\ &\quad + \dots . \end{aligned} \tag{2.10}$$

2.4.2 Expansion of the Numerical Solution

By inserting (**??**) in (**??**), and expanding in Taylor series about u_n, we obtain

$$\begin{aligned} u_{n+1} = \; & u_n + \Delta t \textstyle\sum_{i=1}^{s} b_i f + \Delta t \sum_{i=1}^{s} \hat{b}_i g + \Delta t^2 \sum_{i=1}^{s} b_i \sum_{j=1}^{i-1} a_{ij} f'f \\ & + \Delta t^2 \textstyle\sum_{i=1}^{s} b_i \sum_{j=1}^{i} \hat{a}_{ij} f'g + \Delta t^2 \sum_{i=1}^{s} \hat{b}_i \sum_{j=1}^{i-1} a_{ij} g'f \\ & + \Delta t^2 \textstyle\sum_{i=1}^{s} \hat{b}_i \sum_{j=1}^{i} \hat{a}_{ij} g'g + \dots . \end{aligned} \tag{2.11}$$

An IMEX RK method is said to have order three if, for sufficiently smooth problem as defined in (**??**), and under the assumption that $u_n = u(t_n)$, the local error $u(t_n+\Delta t) - u_{n+1}$ satisfies:

$$u(t_n+\Delta t) - u_{n+1} = \mathcal{O}(\Delta t^4). \tag{2.12}$$

By comparing the exact solution in (**??**) with the numerical approximation in (**??**) and matching the corresponding terms in their Taylor series expansions up to the third order, the necessary conditions for the numerical method to attain third-order accuracy can be established. These conditions ensure that the local truncation error is of order $\mathcal{O}(\Delta t^4)$, thereby guaranteeing that the global error is consistent with a third-order method. The derivation of these conditions can be conveniently expressed through Butcher's rooted tree formalism, which provides a systematic framework for representing and analysing the order conditions of Runge–Kutta-type schemes using P-trees (see Hairer et al., 2009). The resulting order conditions are summarised in the following theorem.

[Order Conditions] The IMEX RK method is of order 3 if the conditions in Tables **??** to **??** are satisfied.

Tree (τ)	$\rho(\tau)$	$\mathcal{F}(\tau)(u_n)$	Order condition(s)	No.
	1	f	$\sum_{i=1}^{s} b_i = 1$	1
	2	$f'f$	$\sum_{i=1}^{s} b_i \sum_{j=1}^{i-1} a_{ij} = \frac{1}{2}$	2
	3	$f'f'f$	$\sum_{i=1}^{s} b_i \sum_{j=1}^{i-1} a_{ij} \sum_{j=1}^{i-1} a_{jk} = \frac{1}{6}$	3
	4	$f''(f,f)$	$\sum_{i=1}^{s} b_i \left(\sum_{j=1}^{i-1} a_{ij}\right)^2 = \frac{1}{3}$	4

Table 1: Rooted trees for the explicit method with black root

Tree (τ)	$\rho(\tau)$	$\mathcal{F}(\tau)(u_n)$	Order condition(s)	No.
	1	g	$\sum_{i=1}^{s} \hat{b}_i = 1$	1
	2	$g'g$	$\sum_{i=1}^{s} \hat{b}_i \sum_{j=1}^{i} \hat{a}_{ij} = \frac{1}{2}$	2
	3	$g'g'g$	$\sum_{i=1}^{s} \hat{b}_i \sum_{j=1}^{i} \hat{a}_{ij} \sum_{j=1}^{i} \hat{a}_{jk} = \frac{1}{6}$	3
	4	$g''(g,g)$	$\sum_{i=1}^{s} \hat{b}_i \left(\sum_{j=1}^{i} \hat{a}_{ij}\right)^2 = \frac{1}{3}$	4

Table 2: Rooted trees for the implicit method with white root

Tree (τ)	$\rho(\tau)$	$\mathcal{F}(\tau)(u_n)$	Order condition(s)	No.
	2	$f'g$	$\sum_{i=1}^{s} b_i \sum_{i=1}^{i} \hat{a}_{ij} = \frac{1}{2}$	1
	3	$f'f'g$	$\sum_{i=1}^{s} b_i \sum_{j=1}^{i-1} a_{ij} \sum_{j=1}^{i} \hat{a}_{jk} = \frac{1}{6}$	2
	3	$f'g'f$	$\sum_{i=1}^{s} b_i \sum_{j=1}^{i} \hat{a}_{ij} \sum_{j=1}^{i-1} a_{jk} = \frac{1}{6}$	3
	3	$f'g'g$	$\sum_{i=1}^{s} b_i \sum_{j=1}^{i} \hat{a}_{ij} \sum_{j=1}^{i} \hat{a}_{jk} = \frac{1}{6}$	4
	3	$f''(f,g)$	$\sum_{i=1}^{s} b_i \sum_{j=1}^{i-1} a_{ij} \sum_{j=1}^{i} \hat{a}_{ij} = \frac{1}{3}$	5
	3	$f''(g,g)$	$\sum_{i=1}^{s} b_i \left(\sum_{j=1}^{i} \hat{a}_{ij} \right)^2 = \frac{1}{3}$	6

Table 3: Rooted trees for the coupling conditions with black trees

Tree (τ)	$\rho(\tau)$	$\mathcal{F}(\tau)(u_n)$	Order condition(s)	No.
	2	$g'f$	$\sum_{i=1}^{s} \hat{b}_i \sum_{j=1}^{i-1} a_{ij} = \frac{1}{2}$	7
	3	$g'g'f$	$\sum_{i=1}^{s} \hat{b}_i \sum_{j=1}^{i} \hat{a}_{ij} \sum_{j=1}^{i-1} a_{jk} = \frac{1}{6}$	8
	3	$g'f'g$	$\sum_{i=1}^{s} \hat{b}_i \sum_{j=1}^{i-1} a_{ij} \sum_{j=1}^{i} \hat{a}_{jk} = \frac{1}{6}$	9
	3	$g'f'f$	$\sum_{i=1}^{s} \hat{b}_i \sum_{j=1}^{i-1} a_{ij} \sum_{j=1}^{i-1} a_{jk} = \frac{1}{6}$	10
	3	$g''(g,f)$	$\sum_{i=1}^{s} \hat{b}_i \sum_{j=1}^{i} \hat{a}_{ij} \sum_{j=1}^{i-1} a_{ij} = \frac{1}{3}$	11
	3	$g''(f,f)$	$\sum_{i=1}^{s} \hat{b}_i \left(\sum_{j=1}^{i} a_{ij} \right)^2 = \frac{1}{3}$	12

Table 4: Rooted trees for the coupling conditions with white trees

We remark here that as the order of the method increases, the number of order conditions increases rapidly and for this reason, we use the simplest simplifying assumptions $\sum_{j=1}^{i-1} a_{ij} = c_i$ and $\sum_{j=1}^{i} \hat{a}_{ij} = c_i$ for the explicit and implicit parts, respectively. It is expected that the order conditions is reduced significantly to enable the easy determination of coefficients as used in the next section for the construction of the methods.

3 Construction of the time-integrators

3.1 IMEX Trapezoidal Method (`IMEX2s2`)

In this subsection, we present the derivation of the IMEX Trapezoidal Method. The Butcher tableau for this method takes the form

$$\begin{array}{c|cc||cc} 0 & 0 & 0 & 0 & 0 \\ c_2 & a_{21} & 0 & \hat{a}_{21} & \hat{a}_{22} \\ \hline & b_1 & b_2 & \hat{b}_1 & \hat{b}_2. \end{array}$$

To ensure that the method achoeves, the order conditions for the explicit component are given by

$$b_1 + b_2 = 1, \tag{3.1a}$$

$$b_1 c_1 + b_2 c_2 = \frac{1}{2}. \tag{3.1b}$$

By taking $c_1 = 0$, we solve (**??**) and (**??**) for b_1 and b_2 to obtain

$$b_1 = 1 - \frac{1}{2c_2}, \qquad b_2 = \frac{1}{2c_2}. \tag{3.2}$$

Similarly, for the implicit component of the IMEX Trapezoidal method, the necessary order conditions are:

$$\hat{b}_1 + \hat{b}_2 = 1, \tag{3.3a}$$

$$\hat{b}_1 c_1 + \hat{b}_2 c_2 = \frac{1}{2}. \tag{3.3b}$$

Solving these equations for $\hat{b}_1$ and $\hat{b}_2$ using (**??**) and (**??**), we obtain

$$\hat{b}_1 = \frac{1}{2}\left(\frac{1 - 2c_2}{c_1 - c_2}\right), \qquad \hat{b}_2 = \frac{1}{2}\left(\frac{2c_1 - 1}{c_1 - c_2}\right). \tag{3.4}$$

We update the Butcher's tableau with the newly derived values

Choosing $c_2 = 1$ and $\hat{a}_{21} = \frac{1}{2}$, we derive the IMEX Trapezoidal Runge-Kutta method, Koto (2008), which is represented by the following Butcher tableau:

$$\begin{array}{c|cc||cc} 0 & 0 & 0 & 0 & 0 \\ c_2 & c_2 & 0 & \hat{a_{21}} & c_2 - \hat{a}_{21} \\ \hline & 1 - \dfrac{1}{2c_2} & \dfrac{1}{2c_2} & \dfrac{1}{2}\left(\dfrac{1-c_2}{c_1-c_2}\right) & \dfrac{1}{2}\left(\dfrac{2c_1-1}{c_1-c_2}\right) \end{array}.$$

$$\begin{array}{c|cc||cc} 0 & 0 & 0 & 0 & 0 \\ 1 & 1 & 0 & \frac{1}{2} & \frac{1}{2} \\ \hline & \frac{1}{2} & \frac{1}{2} & \frac{1}{2} & \frac{1}{2} \end{array}.$$

3.2 3-stage third order methods (IMEX3s3)

We will now derive a three stage 3-stage, third order IMEX Runge-Kutta methods, denoted as IMEX3s3. The coefficients of both the implicit and explicit parts of the scheme are represented using the Butcher tableau:

$$\begin{array}{c|ccc||ccc} c_1 & & & & & & \\ c_2 & a_{21} & & & \hat{a}_{21} & \hat{a}_{22} & \\ c_3 & a_{31} & a_{32} & & \hat{a}_{31} & \hat{a}_{32} & \hat{a}_{33} \\ \hline & b_1 & b_2 & b_3 & \hat{b}_1 & \hat{b}_2 & \hat{b}_3 \end{array}.$$

Let $c_1 = 0$, the third order conditions for the explicit component of the IMEX3s3 are given by the following equations:

$$b_1 + b_2 + b_3 = 1, \tag{3.5a}$$

$$b_2 c_2 + b_3 c_3 = \frac{1}{2}, \tag{3.5b}$$

$$b_3 a_{32} c_2 = \frac{1}{6}, \tag{3.5c}$$

$$b_2 c_2^2 + b_3 c_3^2 = \frac{1}{3}. \tag{3.5d}$$

To simplify the construction, we employ the simplifying assumptions

$$\sum_{j=1}^{i-1} a_{ij} = c_i, \tag{3.6}$$

which ensure consistency between the stage coefficients and the abscissae.

We first solve (**??**) and (**??**) simultaneously for b_2 and b_3 to obtain

$$b_2 = \frac{1}{6}\left(\frac{2 - 3c_3}{c_2(c_2 - c_3)}\right), \qquad b_3 = \frac{1}{6}\left(\frac{3c_2 - 2}{c_3(c_2 - c_3)}\right). \tag{3.7}$$

Substituting b_2 and b_3 into (**??**) to find b_1, gives

$$b_1 = \frac{1}{6}\left(\frac{6c_2c_3 - 3c_2 - 3c_3 + 2}{c_3c_2}\right). \tag{3.8}$$

Next, from (**??**), we find a_{32}:

$$a_{32} = \frac{c_3(c_2 - c_3)}{(3c_2 - 2)c_2}. \tag{3.9}$$

Using the simplifying assumption (**??**) for $i = 3$, we obtain

$$a_{31} = \frac{c_3(3c_2^2 - 3c_2 + c_3)}{3c_2^2 - 2c_2}. \tag{3.10}$$

Similarly, the order conditions for the implicit component of the `IMEX3s3` are listed as follows:

$$\hat{b}_1 + \hat{b}_2 + \hat{b}_3 = 1, \tag{3.11a}$$

$$\hat{b}_2c_2 + \hat{b}_3c_3 = \frac{1}{2}, \tag{3.11b}$$

$$\hat{b}_2\hat{a}_{22}c_2 + \hat{b}_3\hat{a}_{32}c_2 + \hat{b}_3\hat{a}_{33}c_3 = \frac{1}{6}, \tag{3.11c}$$

$$\hat{b}_2c_2^2 + \hat{b}_3c_3^2 = \frac{1}{3}, \tag{3.11d}$$

with the simplifying assumptions $\sum_{i=1}^{i} \hat{a}_{ij} = c_i$, $i = 1, 2, 3$.

Solving (**??**) and (**??**) simultaneously yields

$$\hat{b}_2 = \frac{1}{6}\left(\frac{2 - 3c_3}{(c_2 - c_3)c_2}\right), \qquad \hat{b}_3 = \frac{1}{6}\left(\frac{3c_2 - 2}{c_3(c_2 - c_3)}\right). \tag{3.12}$$

Substituting $\hat{b}_2$ and $\hat{b}_3$ into (**??**) gives

$$\hat{b}_1 = \frac{1}{6}\left(\frac{6c_2c_3 - 3c_2 - 3c_3 + 2}{c_3c_2}\right). \tag{3.13}$$

Using the simplifying assumption, substituting $\hat{b}_1$, $\hat{b}_2$ and $\hat{b}_3$ in (**??**) and (**??**) allows us to determine $\hat{a}_{32}$ and $\hat{a}_{33}$ given by

$$\hat{a}_{32} = \frac{c_3(-3\hat{a}_{21}c_3 + 3\hat{a}_{31}c_2 + 2\hat{a}_{21} - 2\hat{a}_{31} - c_2 + c_3)}{(-2 + 3c_2)(c_2 - c_3)},$$
$$\hat{a}_{33} = \frac{(3c_3 - 3\hat{a}_{31})c_2^2 + (-3c_3^2 + 2\hat{a}_{31} - c_3)c_2 + (3\hat{a}_{21} + 1)c_3^2 - 2c_3^2\hat{a}_{21}}{(-2 + 3c_2)(c_2 - c_3)}.$$

Next, we consider the coupling conditions based on the simplifying assumptions and require that the coefficients obtained so far satisfies the following:

$$b_2\hat{a}_{22}c_2 + b_3\hat{a}_{32}c_2 + b_3\hat{a}_{33}c_3 = \frac{1}{6}, \tag{3.15a}$$

$$\hat{b}_2 a_{22}c_2 + \hat{b}_3 a_{32}c_2 + \hat{b}_3 a_{33}c_3 = \frac{1}{6}. \tag{3.15b}$$

Fortunately, these coupling conditions are automatically satisfied by the coefficients that fulfil the order conditions of both the explicit and implicit parts. Hence, we therefore proceed to construct specific methods based on the choice of the quadrature nodes, see Koto (2008).

Equal Quadratures: $c_2 = \frac{1}{2}$, $c_3 = 1$ **(IMEX3s3a)**

Choosing equal quadratures $c_2 = \frac{1}{2}$, $c_3 = 1$, $\hat{a}_{21} = -\frac{\sqrt{3}}{6}$ and $\hat{a}_{31} = \frac{3}{2} + \frac{5}{6}\sqrt{3}$ results in a three-stage IMEX Runge-Kutta method represented by the Butcher's tableau

$$\begin{array}{c|ccc||ccc}
0 & 0 & 0 & 0 & 0 & 0 & 0 \\
\frac{1}{2} & \frac{1}{2} & 0 & 0 & \frac{-\beta}{2} & \frac{1+\beta}{2} & 0 \\
1 & -1 & 2 & 0 & \frac{3+5\beta}{2} & -(1+3\beta) & \frac{1+\beta}{2} \\
\hline
 & \frac{1}{6} & \frac{2}{3} & \frac{1}{3} & \frac{1}{6} & \frac{2}{3} & \frac{1}{6},
\end{array} \qquad \beta = \frac{\sqrt{3}}{3} \tag{3.16}$$

This method will be referred to as `IMEX3s3a`.

Symmetric Quadratures: $c_3 = 1 - c_2$ **(IMEX3s3b)**

Choosing symmetric quadratures with $c_2 = \dfrac{3+\sqrt{6}}{6}$, $c_3 = 1 - c_2$, $\hat{a}_{21} = 0$ and $\hat{a}_{31} = 1 - 2c_2$ results in a three-stage IMEX Runge-Kutta method represented by the Butcher's tableau:

$$\begin{array}{c|ccc||ccc} 0 & 0 & 0 & 0 & 0 & 0 & 0 \\ \gamma & \gamma & 0 & 0 & 0 & \gamma & 0 \\ 1-\gamma & \gamma-1 & 2(1-\gamma) & 0 & 0 & 1-2\gamma & \gamma \\ \hline & 0 & \frac{1}{2} & \frac{1}{2} & 0 & \frac{1}{2} & \frac{1}{2}, \end{array} \qquad \gamma = \frac{3+\sqrt{3}}{6} \tag{3.17}$$

This method will be referred to as `IMEX3s3b`.

4 Stability region of the IMEX Runge-Kutta Methods

The asymptotic behaviour of numerical solutions to the equation (**??**) is examined as presented in Koto (2008) for the scalar test equation

$$\frac{du}{dt} = \mu u + \lambda u. \tag{4.1}$$

Applying the IMEX scheme to the test equation (**??**) results in

$$U_n = u_n + \Delta t \mu A U_n + \Delta t \lambda \hat{A} U_n, \tag{4.2}$$

$$u_{n+1} = u_n + \Delta t \mu b^T U_n + \Delta t \lambda \hat{b}^T U_n, \tag{4.3}$$

where $U_n \in \mathbb{C}^s$ is an intermediate variable. Solving yields the difference equation

$$u_{n+1} = R(\alpha, z) u_n, \qquad \alpha = \Delta t \lambda, \quad z = \Delta t \mu \tag{4.4}$$

where $R(\alpha, z)$ is defined by

$$R(\alpha, z) = \frac{\det(I - zA - \alpha\hat{A} + zb^T I + \alpha\hat{b} I)}{\det(I - \alpha A)}. \tag{4.5}$$

The function $R(\alpha, z)$ serves as analogue of the stability function of the usual Runge-Kutta method. [Stability of IMEX Runge-Kutta method] Let $R(\alpha, z)$ denote the stability function

associated with an IMEX Runge-Kutta method. The stability region of the method is defined as

$$S = (\alpha, z) \in \mathbb{C}^2 : | \quad R(\alpha, z)| < 1. \tag{4.6}$$

This region comprises all pairs of parameters (α, z) for which the numerical solution remains bounded as the computation proceeds. The geometric structure of this region in the complex plane is generally difficult to visualize. However, for problems, where the eigenvalues of the Jacobian of the f and g are both real, the asymptotic behaviour of numerical solutions is characterized by the restricted region:

$$S^{real} = S \cap \mathbb{R}^2 \tag{4.7}$$

which is easily visualized.

We present in Figure **??**, the stability plots for all the derived methods in the $[-10, 10]^2$ region.

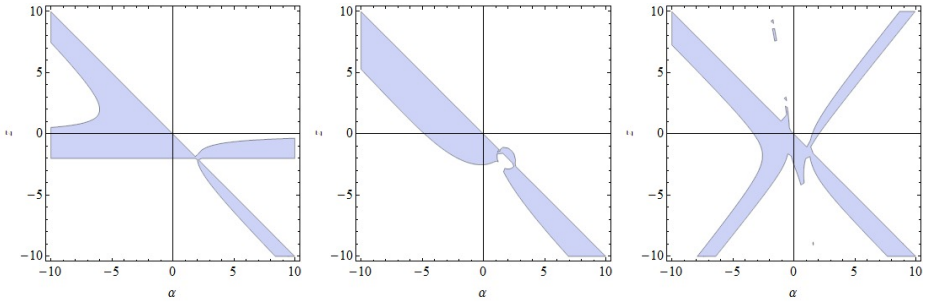

Figure 2: Stability Plot for `IMEX2s2`, `IMEX3s3a` and `IMEX3s3b`

5 Numerical results

Consider a factory located at the center of a 15km by 15km domain. The pollutants, emitted into the atmosphere are influenced by wind speed, random molecular motion, removal (σ) and chemical decay for the reaction term. To study these dynamics, we examine various scenarios that highlight the influence of the parameters of the ADR model (**??**). Specifically, we investigate how diffusion, drift velocity and reaction rates affects the time evolution of the polluted zones.

For this purpose, we simulate the ADR on a uniform grid of size of $(M = 5)$. The computational domain us rectangular and two-dimensional, representing the dispersion of pollutants emitted from a point source located at the centre. The pollutant cocentration

is modelled by the ADR equations with the following parameters:

- Advection velocities: $v\mathrm{km/hr}$
- Diffusion coefficients: $D\mathrm{km}^2/\mathrm{hr}$
- Reaction rate: ($R(u) = -\lambda u$), ($\lambda\mathrm{hr}^{-1}$)
- Transformation coefficient: (σu), ($\sigma\mathrm{km}^{-1}$)

We solve the problem on $\Omega = [0, 15km] \times [0, 15km]$, with the initial pollutant concentration represented by a Gaussian pulse $u_0 = \exp(-(x - M/2)^2 + (y - M/2)^2)$ at the centre of the domain and zero flux at all boundaries to prevent artificial inflow or outflow of pollutants. The accuracy of the methods are investigated using timesteps $\Delta t = \frac{1}{2^j \times 100}, \quad j = 0, 1, 2, 3$. Results are compared across all IMEX Runge-Kutta methods derived in section **??** and with a third-order DIRK method proposed in Kennedy and Carpenter (2019).

5.1 Accuracy

The numerical experiments obtained across all the methods are presented in Table **??**, which reports the maximum global error for different timesteps (Δt).

	`ESDIRK4s3`	`IMEX2s2`	`IMEX3s3a`	`IMEX3s3b`
Δt	$\|u - u_n\|_\infty$	$\|u - u_n\|_\infty$	$\|u - u_n\|_\infty$	$\|u - u_n\|_\infty$
$\frac{1}{100}$	3.15×10^{-1}	3.11×10^{-4}	2.08×10^{-6}	2.08×10^{-6}
$\frac{1}{200}$	1.28×10^{-1}	7.76×10^{-5}	2.61×10^{-7}	2.61×10^{-7}
$\frac{1}{400}$	5.76×10^{-2}	1.94×10^{-5}	3.26×10^{-8}	3.26×10^{-8}
$\frac{1}{800}$	2.74×10^{-2}	4.84×10^{-6}	4.07×10^{-9}	4.07×10^{-9}

Table 5: Maximum global error for all the methods

As shown in Table **??**, the `ESDIRK4s3` method consistently produces the largest global errors, indicating the lowest level of accuracy among the schemes tested. The `IMEX2s2` method performs moderately better, achieving noticeable improvements in accuracy across all time step sizes.

In contrast, the `IMEX3s3a` and `IMEX3s3b` methods exhibit superior accuracy, maintaining error levels that are several orders of magnitude smaller than those of the other schemes. Interestingly, both `IMEX3s3a` and `IMEX3s3b` yield identical numerical results for

all the tested time step sizes, suggesting that the two variants are functionally equivalent in terms of their accuracy.

These results demonstrate the effectiveness of the proposed third-order IMEX Runge–Kutta methods in producing highly accurate solutions even with relatively large time steps, thereby confirming their suitability for solving ADR problems efficiently.

5.2 Numerical Simulation and estimation of pollutant concentration

Finally, we present some simulation results to investigate the effect of the diffusion parameter D.

Influence of drift-velocity and diffusion

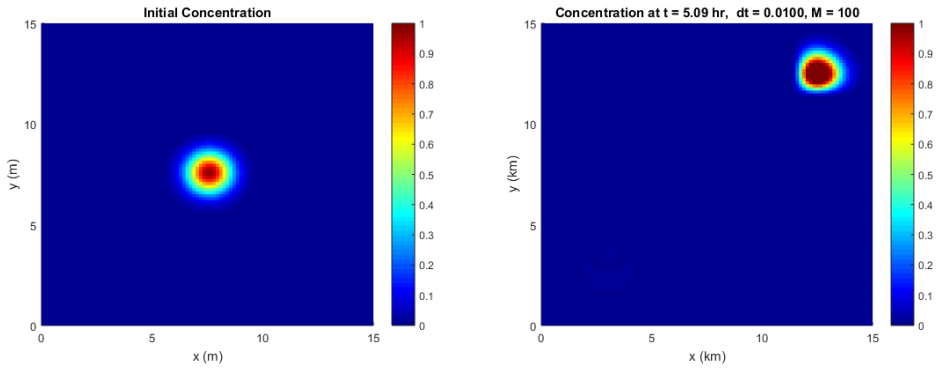

Figure 3: The evolution of the pollutant zones with low diffusion coefficients $D = 0.02\text{km}^2/\text{hr}$ and low dirft-velocity $v = [1, 1]$. The polluted zones at the initial time $t = 0$ and $t = 5.09hr$

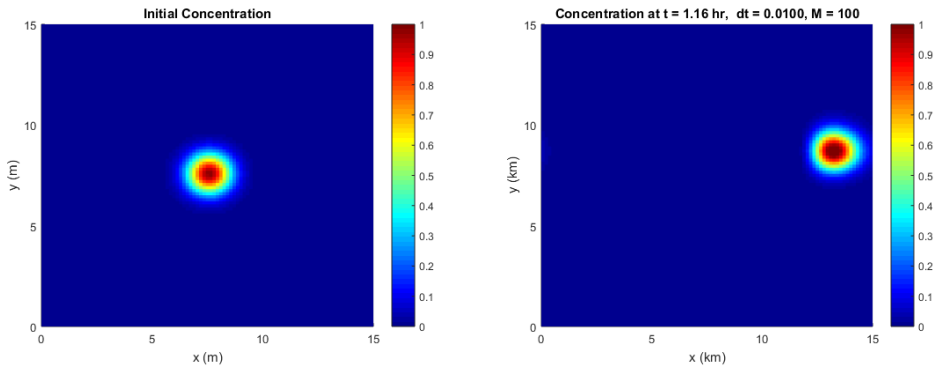

Figure 4: The evolution of the pollutant zones with low diffusion coefficients $D = 0.02\text{km}^2/\text{hr}$ and mixed drift-velocity $v = [1, 5]$. The polluted zones at the initial time $t = 0hr$ and $t = 1.16hr$

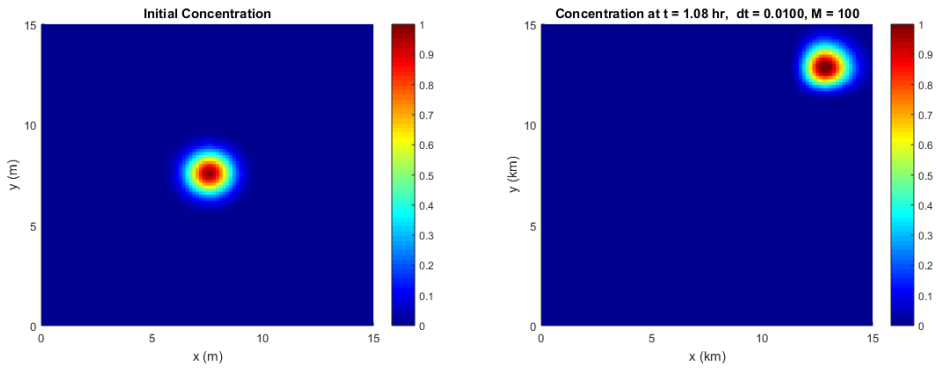

Figure 5: The evolution of the pollutant zones with low diffusion coefficients $D = 0.02\text{km}^2/\text{hr}$ and mixed drift-velocity $v = [5, 5]$. The polluted zones at the initial time $t = 0hr$ and $t = 1.08hr$

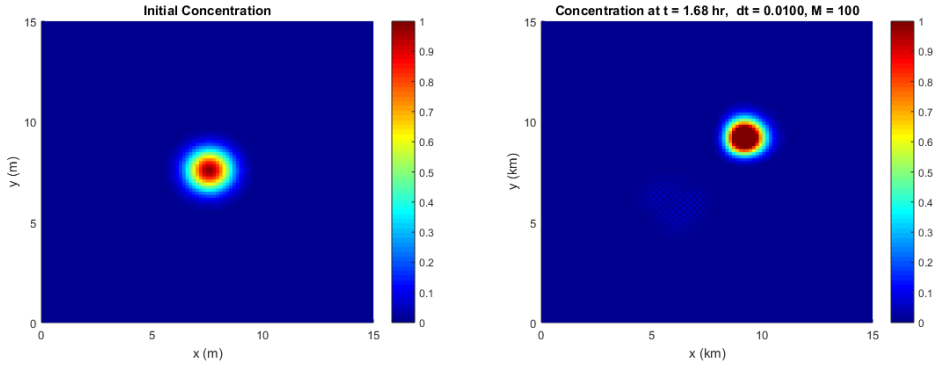

Figure 6: The evolution of the pollutant zones with low diffusion coefficients $D = 0.06\text{km}^2/\text{hr}$ and low dirft-velocity $v = [1, 1]$. The polluted zones at the initial time $t = 0$ and $t = 1.68hr$

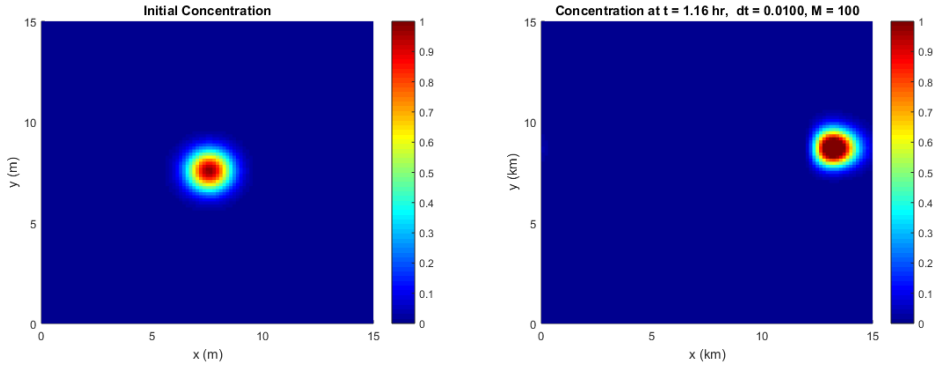

Figure 7: The evolution of the pollutant zones with low diffusion coefficients $D = 0.06\text{km}^2/\text{hr}$ and mixed drift-velocity $v = [1, 5]$. The polluted zones at the initial time $t = 0hr$ and $t = 1.16hr$

Influence of reaction rate and transformation coefficients

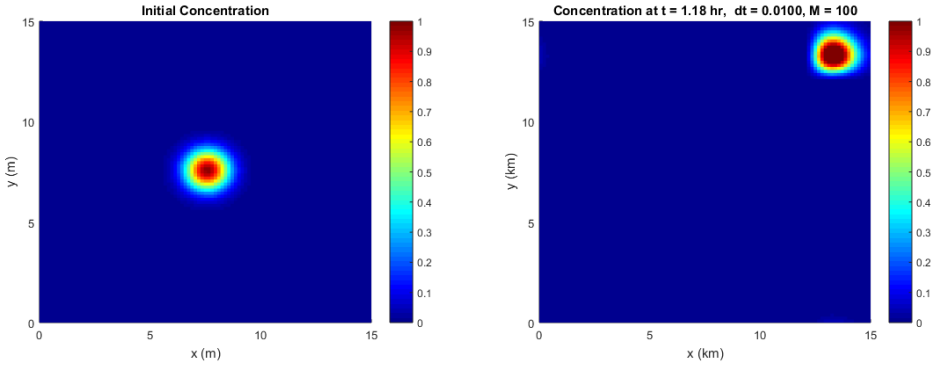

Figure 8: The evolution of the pollutant zones with low diffusion coefficients $D = 0.06\text{km}^2/\text{hr}$ and mixed drift-velocity $v = [5, 5]$. The polluted zones at the initial time $t = 0hr$ and $t = 1.18hr$

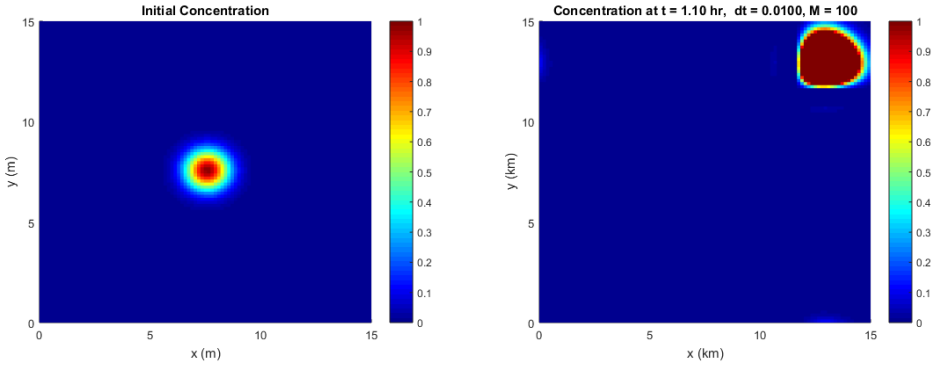

Figure 9: The evolution of the pollutant zones $\lambda = 0.02$ and $\sigma = 2$. The polluted zones at the initial time $t = 0hr$ and $t = 1.10hr$

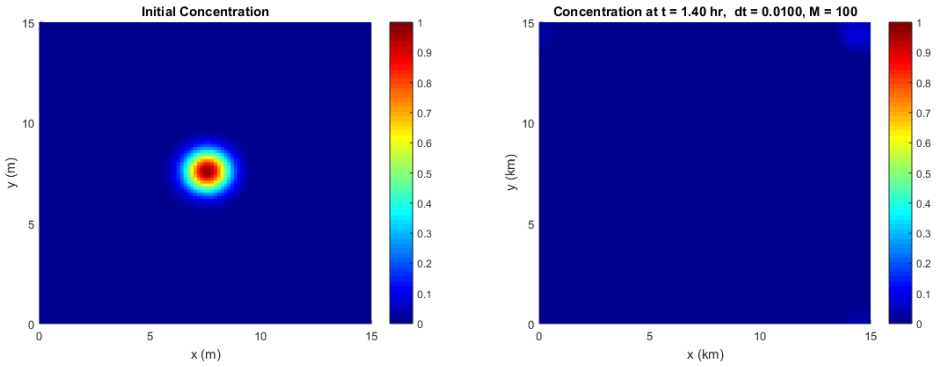

Figure 10: The evolution of the pollutant zones $\lambda = 2$ and $\sigma = 0.02$. The polluted zones at the initial time $t = 0hr$ and $t = 1.14hr$

This subsection has successfully demonstrated the transport and diffusion of pollutants from their initial state to the final time step, taking into account removal and decay parameters of the reaction term. The simulations clearly illustrate how these parameters influence the spatial and temporal evolution of pollutant concentration within the domain. The graphical results reveal the dynamic behaviour of the pollutants as they are advected, diffused, and transformed under different environmental conditions. These

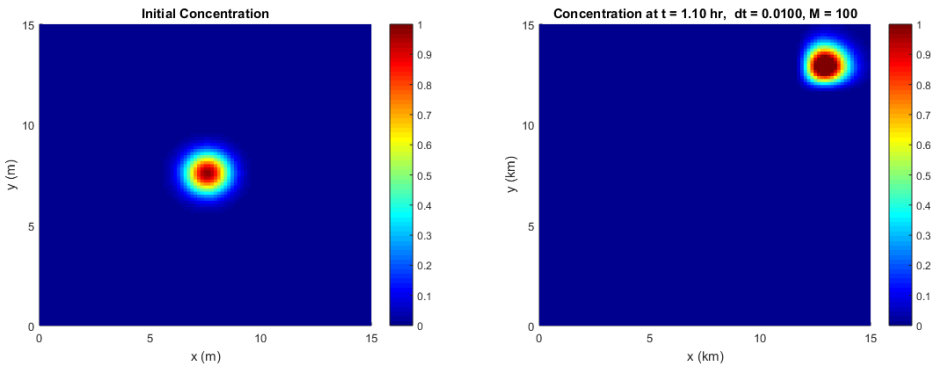

Figure 11: The evolution of the pollutant zones $\lambda = 0.02$ and $\sigma = 0.02$. The polluted zones at the initial time $t = 0hr$ and $t = t = 1.10hr$

findings confirm that the proposed numerical scheme is capable of accurately capturing and tracking the movement and dispersion of pollutants over time, thereby providing valuable insights into how diffusion, advection, and reaction processes interact in air-pollution modelling.

6 Conclusion

This study has presented the development and analysis of efficient Implicit–Explicit (IMEX) Runge–Kutta time-integrators for the numerical simulation of air pollution tracking models governed by advection–diffusion–reaction equations. mathematical model for air-pollution tracking incorporating transport, diffusion, and chemical transformation processes was introduced. The construction of IMEX schemes: the two-stage second-order IMEX Trapezoidal method (`IMEX2s2`) and the three-stage third-order method (`IMEX3s3`), guided by order and coupling conditions ensuring accuracy and consistency between the explicit and implicit components.

The stability region of the methods were presented. Numerical experiments demonstrated that both `IMEX2s2` and `IMEX3s3` accurately reproduced pollutant concentration profiles, with `IMEX3s3` showing enhanced accuracy relative to the `IMEX2s2` and `ESDIRK4s3` method presented in Kennedy and Carpenter (2019). The results confirmed that the proposed IMEX schemes effectively capture the temporal evolution and spatial distribution of pollutants under varying physical and chemical conditions.

Overall, the work provides a computationally efficient framework for real-time air pollution tracking and concentration estimation. The proposed IMEX Runge–Kutta methods can be integrated with data-driven air-quality monitoring platforms to support environmental decision-making and policy development. Future work will focus on incorpo-

rating air-pollution data, applying appropriate boundary conditions in three dimensions, and enhancing the implementation of the implicit component using Newton's technique for more efficient numerical urban air-quality dynamics.

Acknowledgements

J.O. Ehigie and S.A. Okunuga fully acknowledge the University of Lagos and the TET-Fund NRF under the Grant TETF/ES/DR&D-CE/NRF2024/CC/EHU/00072 for the opportunity to conduct this research successfully. The authors thank the reviewers for helpful comments on an earlier draft of this paper.

References

[1] Ahmad, F., Majumder, D., Ranjit, R., Gupta, A., & Manhart, M. (2025). Preliminary study on the spread of air-borne pollutants in urban environment: a CFD simulation approach. Scientific Reports, 15(1), 18836.

[2] Ascher, U. M., Ruuth, S. J., & Spiteri, R. J. (1997). Implicit-explicit Runge-Kutta methods for time-dependent partial differential equations. Applied Numerical Mathematics, 25(2-3), 151-167.

[3] Bürger, R., Gavilan, E., Inzunza, D., Mulet, P., & Villada, L. M. (2020). Mathematics, 8(6), 1034.

[4] Butcher, J. C. (2016). Numerical methods for ordinary differential equations. John Wiley & Sons.

[5] Dang, Q. A., & Ehrhardt, M. (2006). Adequate numerical solution of air pollution problems by positive difference schemes on unbounded domains. Mathematical and Computer Modelling, 44(9-10), 834-856.

[6] Dang, Q. A., Ehrhardt, M., Tran, G. L., & Le, D. (2007). On the numerical solution of some problems of environmental pollution. Air pollution research advances, 171-200.

[7] Dimov, I., Kandilarov, J., Todorov, V., & Vulkov, L. (2017). A comparison study of two high accuracy numerical methods for a parabolic system in air pollution modelling. arXiv preprint arXiv:1701.03049.

[8] Georgiev, K., Zlatev, Z., & Lirkov, I. (2023). Development of new high performance computer architectures and improvements in Danish Eulerian model for long range transport of air pollutants. In International Conference on Large-Scale Scientific Computing (pp. 325-334). Cham: Springer Nature Switzerland

[9] Habingabwa, M. E. N., Ndahayo, F., & Berntsson, F. (2012). Air pollution tracking using pdes. Rwanda Journal, 27, 63-69.

[10] Hairer, E., Nørsett, S. P., & Wanner, G. (2009). Solving ordinary differential equations I: Nonstiff Problems, second revised ed., Springer-Verlag, Heidelberg, 2009

[11] Karátson, J., & Kovács, B. (2016). A parallel numerical solution approach for non-linear parabolic systems arising in air pollution transport problems. In Mathematical Problems in Meteorological Modelling (pp. 57-70). Cham: Springer International Publishing.

[12] Kennedy, C. A., & Carpenter, M. H. (2019). Diagonally implicit Runge–Kutta methods for stiff ODEs. Applied Numerical Mathematics, 146, 221-244.

[13] Koto, T. (2008). IMEX Runge–Kutta schemes for reaction–diffusion equations. Journal of Computational and Applied Mathematics, 215(1), 182-195.

[14] Liang, K., Zhu, Y., Liu, J., & Zhang, Q. (2025). A fourth-order cut-cell method for solving the two-dimensional advection-diffusion equation with moving boundaries. arXiv preprint arXiv:2503.16877.

[15] Rodrigo Bonet, E. (2024). Explainable and physics-guided graph deep learning for air pollution modelling. [PhD Thesis, Vrije Universiteit Brussel].

[16] Rubin, H. (2001). Environmental fluid mechanics. CRC Press.

[17] Salman, A. K. (2024). Advanced deep learning frameworks for pollution modeling: applications in numerical solving, model emulation, and uncertainty-aware air quality forecasting (Doctoral dissertation).

[18] Shettar, B. M., Hiremath, P. N., Madhukesh, J. K., Ramesh, G. K., & Ramesha, M. (2024). Aggregation of magnetized nanoparticles (TiO2-EG) across stretching disc with pollutant concentration. Hybrid Advances, 6, 100212.

[19] Wang, Z., Li, J., Wu, L., Zhu, M., Zhang, Y., Ye, Z., & Wang, Z. (2022). Deep learning-based gas-phase chemical kinetics kernel emulator: Application in a global air quality simulation case. Frontiers in Environmental Science, 10, 955980.

[20] Yang, L., Li, T., Wong, S. C., Shu, C. W., & Zhang, M. (2019). Modeling and simulation of urban air pollution from the dispersion of vehicle exhaust: A continuum modeling approach. International Journal of Sustainable Transportation, 13(10), 722-740.

[21] Zlatev, Z., Dimov, I., Faragó, I., Georgiev, K., & Havasi, Á. (2022). Efficient implementation of advanced Richardson Extrapolation in an atmospheric chemical scheme. Journal of Mathematical Chemistry, 60(1), 219-238.